Characterization of the PEO−PPO−PEO Triblock Copolymer and Its Application as a Separation Medium in Capillary Electrophoresis

Chunhung Wu, Tianbo Liu, and Benjamin Chu*

Department of Chemistry, State University of New York at Stony Brook, Stony Brook, New York 11794-3400

Dieter K. Schneider and Vito Graziano

Biology Department, Brookhaven National Laboratory, Upton, New York 11973

Received January 28, 1997; Revised Manuscript Received April 14, 1997[⊗]

ABSTRACT: The Pluronic polyol F127, $PEO_{99}PPO_{69}PEO_{99}$ (PEO and PPO being poly(ethylene oxide) and poly(propylene oxide), respectively) has the potential to be used as an effective separation medium in capillary electrophoresis (CE) for the separation of biomacromolecules such as DNA fragments and proteins. Static light scattering (SLS), dynamic light scattering (DLS), small-angle neutron scattering (SANS), and small-angle X-ray scattering (SAXS) were used to characterize the solution properties and the microstructures of F127 in the same electrophoresis buffer used in CE. In the dilute solution region, F127 in CE buffer forms micelles similar to that in water. At high solution concentrations, micelles tend to pack into some crystalline forms with relatively well-structured PPO centers. By using a combination of SANS and SAXS results, we are able to conclusively determine the gellike structure to have a face-centered cubic lattice. The effects of solvent, polymer concentration, temperature, and sample preparation procedure on the gel structure were studied. In the gellike region the aggregation number and also the micellar size are not sensitive to both the concentration change and the temperature change. The results of DNA electrophoretic migration in F127 gels also support these findings.

Introduction

Triblock copolymers (PEO−PPO−PEO) consisting of a central block of poly(propylene oxide) and end blocks of poly(ethylene oxide) exhibit very interesting physical properties when dissolved in a selective solvent, which is a good solvent for only one of the blocks. The amphiphilic character of the block copolymer leads to self-assembly behavior resembling that of the low molecular weight ionic surfactants and thus finds many industrial applications.[1] The rich-phase behaviors including liquid crystalline gel regions of lamellar, hexagonal, and cubic structures formed by the block copolymers with different chain length, block length ratio, and chain architecture were the subjects of many recent studies.[2−4] In general, the PEO−PPO−PEO triblock copolymer aqueous solution is in a unimer state at low temperatures and low polymer concentration since both blocks (PEO and PPO) are soluble at low temperatures (<15 °C). Increasing the temperature causes an increase in the hydrophobicity of the PPO block and leads to micellar formation. As unimers, the PEO−PPO−PEO triblock copolymers have relatively low molecular weights. Therefore, such a solution behaves like a Newtonian fluid with relatively low viscosity even at fairly high polymer concentrations since the overlap concentration would be unusually high.[5−7] However, at an appropriate concentration and temperature the polymer solution can form micelles which overlap to yield a gellike medium with supramolecular crystalline structures. This thermally reversible "gelation" property along with low toxicity also make it possible for the application of controlled drug delivery.[1]

Capillary electrophoresis with replaceable polymer solution as a sieving medium is a newly developed technique for the separation of biomacromolecules such as DNAs and proteins.[8] It also plays an important role in the high-throughput automated sequencing of genomes.[9] In order to achieve a reasonable separation resolution, viscous polymer solutions at concentrations far in excess of the overlap concentration are usually used.[10] However, the introduction of such a viscous polymer solution into the narrow bore capillary column with an inner diameter of usually not more than 100 μm is not a routine procedure.

By taking advantage of the unique sol−"gel" transition property of PEO−PPO−PEO, a Pluronic polyol F127, $PEO_{99}PPO_{69}PEO_{99}$, was selected as the separation medium for capillary electrophoresis (CE).

Static light scattering (SLS), dynamic light scattering (DLS), small-angle neutron scattering (SANS), and small-angle X-ray scattering (SAXS) were used to characterize the solution properties and the microstructures of F127 in the same electrophoresis buffer used in CE. It was known that F127 aqueous solutions with additives showed altered phase behaviors.[11−14] Although many experiments have been reported on F127 aqueous solutions in both micellar and "gel" regions,[5−7,11−25] discrepancies of the results from different groups did exist.[15] Recent studies of the crystalline gel structure of F127 in aqueous solution by two research groups showed two different cubic lattices.[7,16] Mortensen and Talmon[16] used model fitting for the scattering curves obtained by SANS and showed the shear-aligned cubic pattern of the F127 gel. They concluded that the colloidal crystal of F127 is a body-centered cubic lattice while Prud'homme et al.[7] derived a simple cubic symmetry for the micellar cubic phase of F127 by using SANS and rheology.

Experimental Section

Materials. F127 Solutions. Pluronic F127 solutions were prepared by mixing polymers (a gift from the BASF Corp., Parsippany, NJ) with solvents such as H_2O, 1X TBE buffer

[⊗] Abstract published in *Advance ACS Abstracts,* July 1, 1997.

S0024-9297(97)00108-3 CCC: $14.00

(89 mM tris(hydroxymethyl)aminomethane, 89 mM boric acid, and 2 mM EDTA in deionized water), sequencing buffer (SB, 1X TBE + 3.5 M urea, and 30% formamide), and 1X Tris−glycine buffer (25 mM Tris and 192 mM glycine in deionized water) to desired concentrations (all buffer reagents bought from Sigma Chemical Co.). Before use, all the solvents were filtered by Millipore sterile membrane filters (0.1 μm pore size). The mixture was stirred in an ice bath for at least 1 h. The foamy solution was then stored in the refrigerator at 4 °C for a few days before use. In order to enhance the scattering contrast for SANS experiments, H_2O was replaced by D_2O. In SB, deuterated urea (D_2NCOND_2) was also used. Deuterated materials were bought from Cambridge Isotope Lab., Andover, MA. The F127 solutions for laser light scattering experiments were prepared by diluting a stock solution of 100 mg/mL. Dust-free solutions were obtained by filtering the diluted solutions through Millipore sterile membrane filters (0.1 μm pore size) into 17 mm o.d. cylindrical light-scattering cells, which had been rinsed with distilled acetone.

Fluorescein-Labeled GH5. This is the recombinant fragment of a mutant of the globular domain of histone H5, contains 89 amino acids, and is 9642 Da. Protein samples (∼10 mg/mL) were incubated with an excess of reducing agent dithiothreitol (DTT) for 45 min at room temperature before labeling with 6-iodoacetamidofluorescein (6-IAF). DTT was removed by passing the solution through a Bio-Rad Bio-spin 6 chromatography column. The proteins was covalently labeled with the fluorescent dye 6-IAF by adding a 2-fold molar excess of 6-IAF. The reaction mixture, in 50 mM sodium phosphate buffer, pH 8.0, was incubated in the dark for 60 min at room temperature. Unreacted free fluorescein was removed by passage through several spin columns.

DNA Samples. The DNA size standard sample was purchased from Sigma Chemical Co. *ϕX174* DNA-Hae III digest was purchased from New England Biolabs, Inc. All the DNA samples prepared by restriction enzymes digest were diluted to 10 μg/mL by using the 1X TE buffer (10 mM Tris·HCl + 1 mM EDTA).

Methods. Capillary Electrophoresis (CE). A 13 cm long fused silica capillary (Polymicro Technologies) with ID/OD = 98 μm/364 μm was flushed with 1 mL of 1 N HCl over a period of about 10 min. A detection window of 2-mm width was opened at 10 cm from the cathodic end by stripping the polyimide coating off with a razor blade. Both cathode and anode reservoirs (2.6 mL volume) were filled with a running buffer of 1X TBE and 1 μg/mL ethidium bromide (Sigma Chemical Co.; for DNA analysis only since the protein samples have been labeled with 6-IAF already). The block copolymer solution was filled into the capillary tubing by using a 50 μL syringe at 4 °C. The capillary tubing was then assembled on the capillary electrophoresis apparatus and raised to room temperature. The polymer solution then became gellike over a period of about 10 min. A prerun at constant electric field strength of 200 V/cm for about 25−30 min (depending on the dye electrophoretic mobility in the separation medium) was used to introduce the fluorescent dye (for DNA analysis only) into the separation medium and to stabilize the current. The DNA or protein sample was electrokinetically injected into the capillary tubing at an electric field strength of 300 V/cm or 5 s. The runtime electric field strength was 200 V/cm. Our laboratory-built laser-induced fluorescence capillary electrophoresis instrument used an argon ion laser operating at a wavelength of 488 nm with a 5 mW output power.[26] The fluorescence from the DNA−ethidium bromide complex or the fluorescein-labeled GH5 protein was collected by using a Zeiss epillumination fluorescence microscope and a Hamamatsu R928 photomultiplier tube. Two bandpass emission filters, 605DF50 and 530DF30 (Omega Optical, Bratleboro, VT), were used for the collection of fluorescence signals from the DNA−ethidium complex and the fluorescein−protein complex, respectively. To replace the separation medium, the gellike block copolymer separation medium could be transformed back into a solution by lowering the temperature to 4 °C. The copolymer solution was extruded by using 1 mL of distilled water and then rinsed with 1 mL of 1 N HCl over a period of 10 min before introduction of the new copolymer solution.

Laser Light Scattering (LLS). A laboratory-built laser light scattering spectrometer[27] operating at a wavelength of 514.5 nm with an output power of about 600 mW was used to perform static light scattering (SLS) and dynamic light scattering (DLS) measurements at a scattering angle of 90° over a range of temperatures from 20 to 42 °C. The intensity correlation function was measured by using a Brookhaven BI-2030 digital correlator.

SANS Experiments. SANS experiments were performed by using the small-angle neutron scattering spectrometer located at H9B in the high flux beam reactor (HFBR) of Brookhaven National Laboratory. The wavelength was set at 7.29 Å with a spread in $\Delta\lambda/\lambda$ of about 10%. The sample to detector distance was 175.8 cm. Samples were contained in capped spectroscopic quartz cuvettes of 2 mm path length. The experimental scattering curves were normalized by incident neutron counts. Dark count, sample absorption, solvent scattering, and detector nonlinearity were also taken into account.

SAXS Experiments. SAXS experiments were performed at the X3A2 State University of New York (SUNY) beam line, National Synchrotron Light Source (NSLS) at Brookhaven National Laboratory (BNL), using a laser-aided prealigned pinhole collimator.[28] The incident beam wavelength (λ) was tuned at 0.154 nm. A Fuji imaging plate was used as the detection system. The sample-to-detector distance was 1085 mm. The experimental data were corrected for background scattering and sample transmission. Samples were introduced into glass capillaries with a 2 mm diameter at 4 °C. The capillary tubing was then sealed by a flame.

Results and Discussion

Application of F127 Solution on Capillary Electrophoresis. According to the empirical rule,[29] the PEO−PPO−PEO block copolymer will not form a gel if the molecular weight of the hydrophobe is less than 1750 (∼30 PO units). Moreover, the larger the PPO block and the greater the PEO content, the greater is the gelling ability of the triblock copolymer. Under this kind of consideration, we chose F127 as the test object since it has the lowest gelation concentration at room temperature when compared with existing available Pluronic polyols. Even though PEO could collapse DNA into compact particles[30,31] and the incompatibility property between PEO and protein was used for protein purification,[32] the use of PEO−PPO−PEO triblock copolymer as a separation medium does not seem to show such an effect in our studies. Figure 1 shows the electropherograms of fluorescein-labeled GH5 protein (upper plot (a)) and the DNA size standard (lower plot (b)). Sharp and well-resolved peaks were obtained. It is noted that there exists an anomalous DNA migration (i.e., reversal of 138 and 157 bp fragments) in the small DNA region of the electropherogram. This phenomenon was also found in slab polyacrylamide gel electrophoresis[33] and linear polyacrylamide capillary electrophoresis.[34] The possible reason could be due to DNA sequence dependent conformational change. However there is no sign for either analyte adsorption on the capillary wall or DNA precipitation. Therefore, we have demonstrated that triblock copolymers of PEO−PPO−PEO has the potential for application as a separation medium in capillary electrophoresis.

LLS Study for Dilute F127 Solution in 1X TBE Buffer. By increasing the triblock copolymer concentration or the temperature to a certain value, laser light scattering could measure an abrupt increase in the scattered intensity, signaling the presence of larger micellar particles. The critical micelle concentration is defined as the concentration at which the laser light scattering intensity departs significantly from the base-

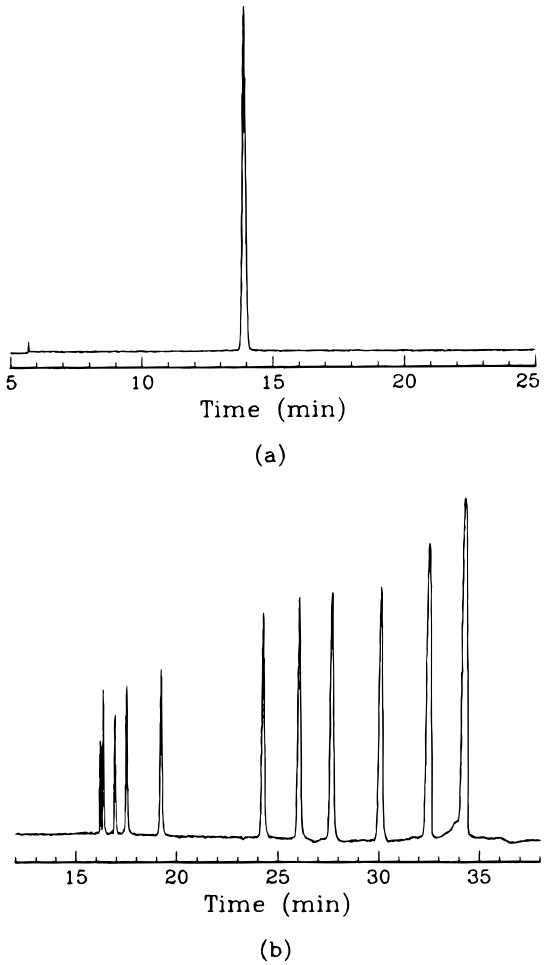

Figure 1. (a) Electropherogram of fluorescein-labeled GH5 protein with a molecular weight of 9642. The small peak at about 5.7 min is due to the free fluorescein dye molecules (b) Electropherogram of a dsDNA size standard sample. Peak identifications from right to left in base pairs are as follows: 1560, 964, 645, 525, 472, 392, 247, 197, 138, 157, and 89 (1 base pair ≈ 649 Da). Electrophoresis conditions are described in the text.

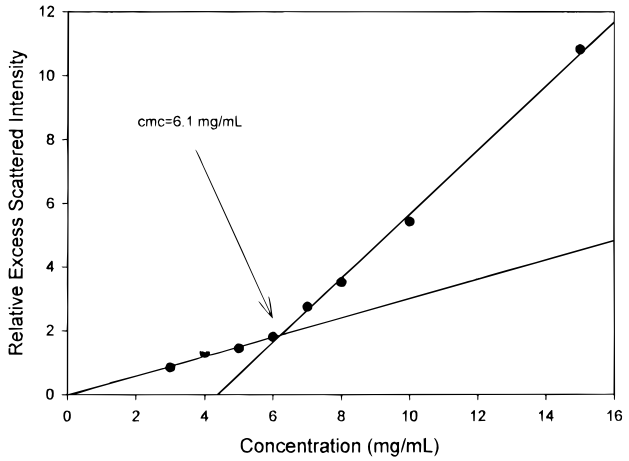

Figure 2. Plot of relative excess scattered intensity at $\theta = 90°$ vs concentration of F127 in 1X TBE buffer solution at 25 °C. The arrow indicates the intersection of two linear regression lines of the scattered intensity. The relative excess scattered intensity I_{ex} was calculated by using the relation $I_{ex} = (I - I_0)/I_{BZ}$, where I, I_0, and I_{BZ} are the scattered intensities of polymer solution, 1X TBE buffer, and benzene, respectively.

line intensity contributed only by unimers. Figure 2 shows a typical SLS result for the determination of the cmc. The cmc value was estimated by the intersection

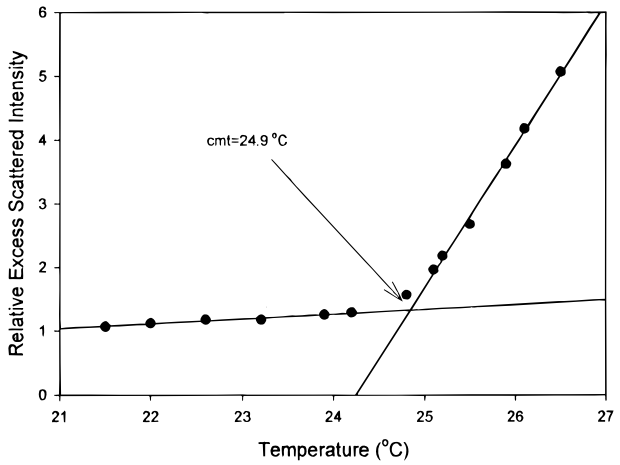

Figure 3. Plot of relative excess scattered intensity vs temperature for a 6.0 mg/mL F127 solution in 1X TBE buffer. Critical micellar temperature (cmt) ≅ 24.9 °C.

Table 1. Critical Micelle Concentration and Aggregation Number N_w of F127 in 1X TBE Buffer Derived from SLS

temp (°C)	cmc (mg/mL)	N_w
20	52.0	2
25	6.1	5
30	0.4	12
35	~0.03	23
40	~0.003	33

of the two linear regression lines with cmc = 6.1 mg/mL for F127 in 1X TBE buffer at 25 °C. The relative excess scattered intensity I_{ex} was calculated by $(I - I_0)/I_{BZ}$, where I, I_0, and I_{BZ} are the scattered intensity of polymer solution, 1X TBE buffer, and benzene, respectively. The cmc values obtained from SLS at different temperatures are listed in Table 1. Due to the low scattered intensity, the baseline scattered intensity due to unimers at 35 and 40 °C is not measured but is estimated from the I_{ex} vs concentration plot measured at lower temperatures. If the temperature dependence of the relative excess scattered intensity of a copolymer solution is followed at a given concentration, the critical micelle temperature (cmt) can be determined by using the same approach as for the cmc determination. Figure 3 shows a plot of I_{ex} vs temperature for a 6 mg/mL solution of F127 in 1X TBE buffer. The cmt value derived for the 6 mg/mL F127 solution in 1X TBE buffer is 24.9 °C, which confirms the cmc value of 6.1 mg/mL at 25 °C as listed in Table 1. The thermodynamic parameter ΔH^0, standard enthalpy of micelle formation, can also be estimated based on the Gibbs−Helmholtz equation:[24]

$$\Delta H^0 = -RT^2[\partial ln(\text{cmc})/\partial T]_p = R[\partial ln(\text{cmc})/\partial(1/T)]_p \quad (1)$$

Figure 4 shows a plot of the logarithmic critical micelle concentration (cmc) against the reciprocal of absolute temperature. From the slope of the least-squares fit, ΔH^0 is derived to be 380 ± 10 kJ/mol.

To calculate the micellar aggregation number, we use the Rayleigh−Gans−Debye equation in the modified form[35]

$$H(\text{c-cmc})/R_{mic,90} = 1/M_w + 2A_2(\text{c-cmc}) \quad (2)$$

where H $(=4\pi n_0^2(dn/dc)^2/N_A\lambda^4)$ is an optical constant with n_0 being the refractive index of solvent, dn/dc is the refractive index increment, N_A is Avogadro's constant, λ is the laser light wavelength (514.5 nm), $R_{mic,90}$

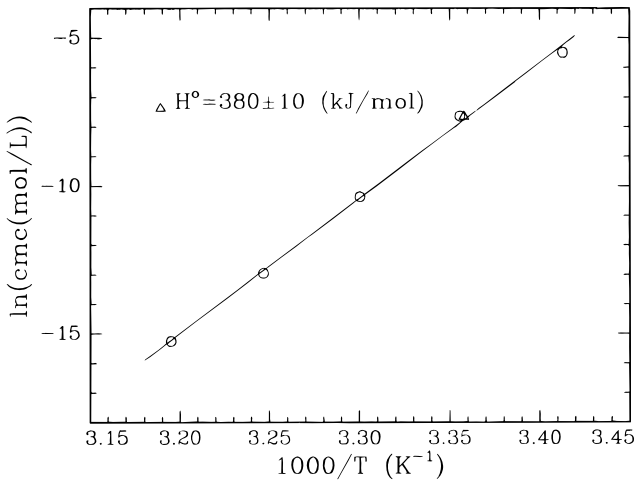

Figure 4. Logarithmic plot of critical micelle concentration (cmc) against reciprocal of absolute temperature: (○) data taken from cmc measurements; (△) data taken from cmt measurement.

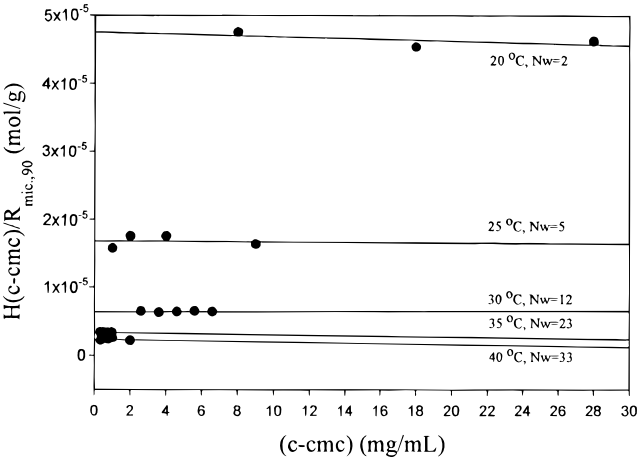

Figure 5. Plot of H(c-cmc)/$R_{mic,90}$ vs c-cmc for F127 in 1X TBE buffer solution at 20, 25, 30, 35 and 40 °C. The aggregation number N_w is calculated from the micellar molecular weight and the initial unimer molecular weight and is listed in Table 1.

(=$R_{BZ,90}$ ($(I - I_{cmc})/I_{BZ}$). n^2/n_{BZ}^2,) is the Rayleigh ratio of micelle at 90° with I_{cmc} being the scattered intensity at cmc and n and n_{BZ} being the refractive index of solution and benzene, respectively, M_w is weight-average molecular weight, and A_2 is the second virial coefficient. A plot of H(c-cmc)/$R_{mic,90}$ vs c-cmc is shown in Figure 5. The micellar weight-average molecular weight at different temperatures can be estimated by extrapolating the c-cmc to zero. The aggregation numbers (N_w) can thus be derived and are listed in Table 1. Increasing the temperature will increase the hydrophobicity of the PPO block and thus induce the micellar formation. The N_w value apparently increases with increasing temperature. This phenomenon was commonly found in the dilute solution regime of the Pluronic polyols.

Dynamic light scattering (DLS) measures the intensity−intensity time correlation function $G^{(2)}(\tau)$, with τ being the delay time. Laplace inversion (we used the CONTIN method[36] for the data analysis) of $G^{(2)}(\tau)$ yields the normalized characteristic line width distribution function $G(\Gamma)$. The characteristic line width Γ can be related to the translational diffusion coefficient D by $D = \Gamma/q^2$, with q being the magnitude of the momentum transfer vector. With the Stokes−Einstein relation which applies in the dilute solution region

$$R_h = k_B T/(6\pi\eta D) \quad (3)$$

where k_B is the Boltzmann constant and η is the solvent viscosity at temperature T, we can determine the equivalent hydrodynamic radius, R_h. Figure 6 shows plots of intensity contribution function $\Gamma G(\Gamma)$ vs the apparent hydrodynamic radius of a 10 mg/mL F127 solution in 1X TBE buffer at four different temperatures. The corresponding average R_h values of both unimers and micelles are listed in Table 2. At 20 °C and 10 mg/mL, F127 exists essentially as unimers with $R_{h,app} = 2.9$ nm. Micelles do not exist at 10 mg/mL since the cmc value for F127 in 1X TBE buffer at 20 °C is 52.0 mg/mL. When the temperature is increased to 25 °C, which has a corresponding cmc value of 6.1 mg/mL, micelles are formed and coexist with unimers whose $R_{h,app}$ value is decreased slightly to 2.4 nm. The average $R_{h,app}$ value for the micelles is about 12 nm. The size of unimers contracts with increasing temperature partly because the solvent quality decreases with increasing temperature. The unimer size distribution also becomes narrower with increasing temperature. When the temperature is increased to 35 °C, the dynamic equilibrium between unimers and micelles is shifted heavily in favor of micelles. Therefore, only the micellar peak is observed in Figure 6c. The $R_{h,app}$ of micelles at 35 °C is about 11.4 nm, which is slightly smaller than that at 25 °C even though the N_w value has grown by a factor of 5. At 25 °C, the small N_w value suggests that the PPO blocks form a core which contains a substantial amount of buffer and has a porous structure. At 35 and 42 °C micelles become more dense both in the core and in the corona. Therefore, although the overall gellike structure remains about the same with temperature, the effective pore sizes within the supramolecular micellar structures have decreased with increasing temperature. It is also noted that the micellar size distribution becomes narrower with increasing temperature as shown schematically in Figure 6b−d. Similar phenomena have been reported in the other Pluronic block copolymer systems.[37] Copolymers with a similar PPO block length but longer PEO blocks also tend to have broader R_h distributions.

SANS and SAXS Studies on F127 Gel Structure. Structural studies on Pluronic gels were usually performed by using SANS or SAXS. However, because of the considerable scattering contrast difference between SANS and SAXS, distinct scattering patterns could be obtained by using a combination of these two methods. Indeed conflicting conclusions could be drawn at times.[38,39] In this study we try to use both methods to investigate the F127 gel structure in order to extract the appropriate information.

SANS. We would like to study the structure of F127 gels in capillary electrophoresis buffers in order to optimize its application as a separation medium for biomacromolecules. Figure 7 shows the SANS intensity profiles of 21.2% (w/v) F127 in D_2O, 1X TBE buffer, and sequencing buffer (SB) at 25 °C obtained by circular integration of the corresponding two dimensional scattering patterns. The scattering curves of F127 in D_2O and in TBE are overlapped together without distinguishable difference. However, in SB solution the F127 scattered intensity is lower than that in D_2O and TBE. This is mainly due to the lower scattering length density in SB caused by the addition of formamide. Therefore the scattering contrast is lowered in SB solution. Beside the difference in the magnitude of the scattered inten-

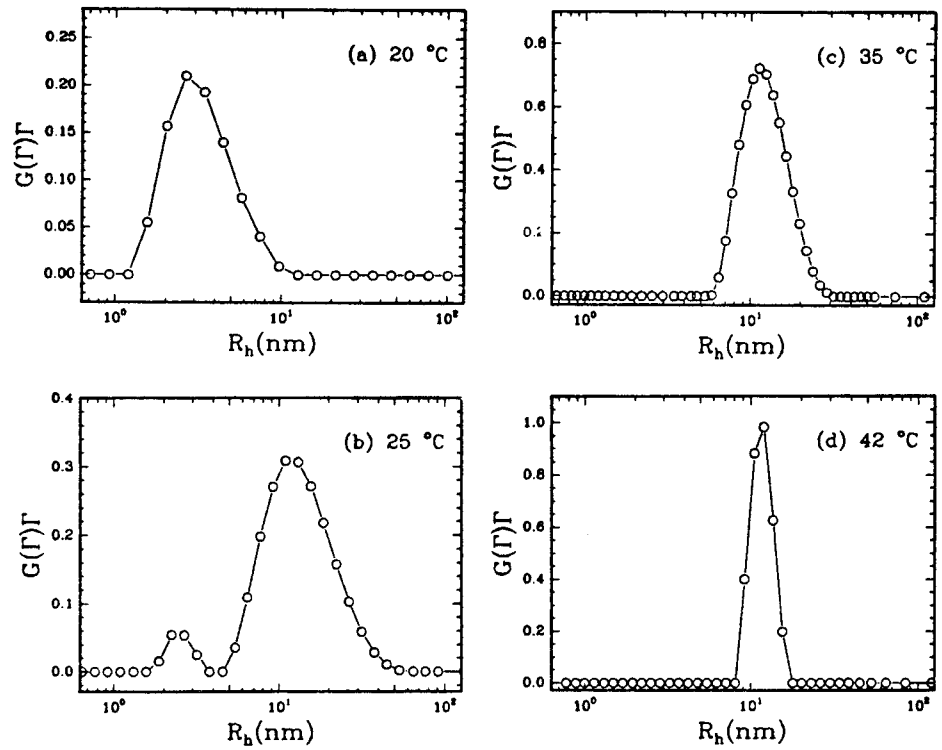

Figure 6. Plots of intensity contribution function $\Gamma G(\Gamma)$ vs apparent hydrodynamic radius R_h of a 10 mg/mL F127 solution in 1X TBE buffer at four different temperatures. The data analysis is based on the CONTIN method. Note: R_h means $R_{h,app}$.

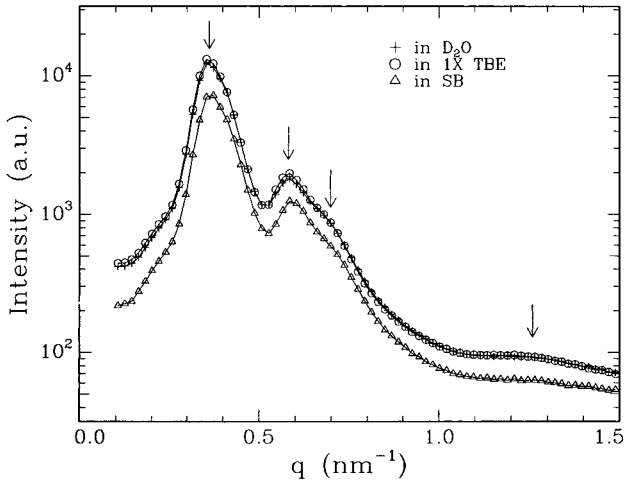

Figure 7. SANS intensity profiles of 21.2% (w/v) F127 in D_2O, 1X TBE buffer, and sequencing buffer (SB) at 25 °C obtained by circular integration of the corresponding two dimensional scattering patterns. The arrows from left to right indicate the peak positions at around 0.36, 0.58, 0.71, and 1.26 nm^{-1}, respectively. The solid lines connecting the data points are for guiding the eyes.

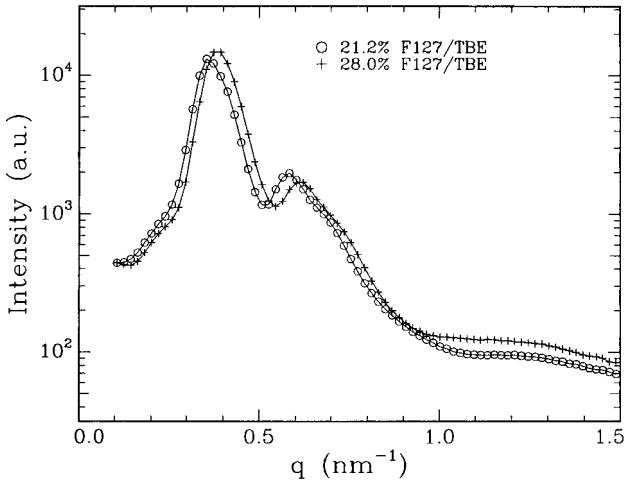

Figure 8. SANS intensity profiles of 21.2% (w/v) and 28.0% (w/v)% F127 in 1X TBE buffer solutions.

Table 2. Average $R_{h,app}$ Values for Unimers and Micelles Obtained from DLS at a F127 Concentration of 10 mg/mL in 1X TBE Buffer

temp (°C)	$R_{h,app}$(unimer) (nm)	$R_{h,app}$(micelle) (nm)
20	2.9	
25	2.4	12.0
35		11.4
42		11.5

sity, the peak positions are very similar. All three scattering curves show a main peak at $q \cong 0.36$ nm^{-1} ($q = 4\pi/\lambda$) $\sin(\theta/2)$), where θ is the scattering angle), a second peak at $q \cong 0.58$ nm^{-1} with a shoulder at $q \cong 0.71$ nm^{-1}, and a very broad shoulder located at q values between 1.1 and 1.4 nm^{-1}. The scattering at small scattering angles is usually attributed to the Bragg diffraction caused by interparticle interference, while the scattering at larger scattering angles is recognized as intraparticle scattering. From the three diffraction peaks, we are not able to determine the structure according to the relative peak positions. However, if we consider the micellar core as a dense sphere with radius R_c, the form factor which describes the intraparticle scattering can lead to the local maxima at $qR_c = 5.77$, 9.10, 12.3, etc.[40] Taking $q \cong 1.26$ nm^{-1}, the micellar core size can thus be estimated as 4.6 ± 0.2 nm. We will examine this value later by using the crystal lattice parameters obtained from the SAXS study.

Figure 8 shows the polymer concentration effect on the F127/TBE gel structure. At the higher polymer concentration, the Bragg diffraction peaks shift to a higher q range, while the broad feature from intraparticle interference seems to remain the same. With a similar scattering pattern but higher q values of dif-

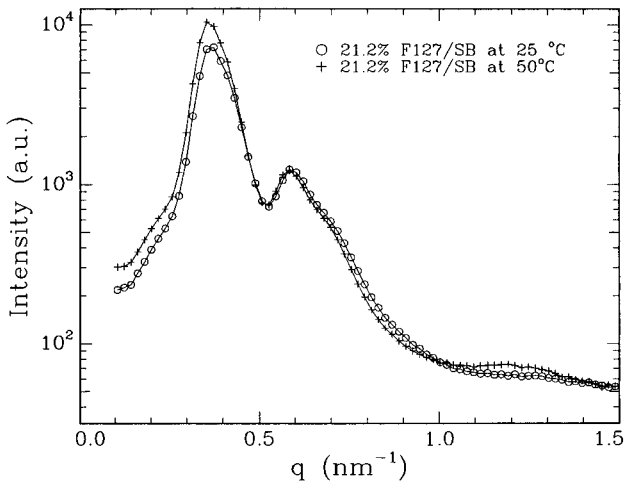

Figure 9. SANS intensity profiles of 21.2% (w/v) F127 in sequencing buffer at 25 and 50 °C, respectively.

fraction peaks and the same form factor, we can qualitatively draw the picture that micelles have the same size at higher polymer concentration; i.e., the aggregation number N_w does not change. Therefore the increased micelle number density results in a higher degree of overlap between the micellar coronas of the PEO blocks. The decreasing intermicellar distance is thus exhibited by a corresponding shift in the diffraction peaks to larger q values. The same concentration effect has been observed in SB solution and in D_2O solution.

The temperature effect on the F127/SB gel structure is shown in Figure 9. The diffraction peak positions remain the same by increasing the temperature from 25 to 50 °C, suggesting that the intermicellar distance is not changed with increasing temperature. Assuming that there is polymer chain exchange between micelles in the gel state and that increasing temperature will increase the aggregation number as observed in dilute solution by LLS, then the amount of micelles will decrease dramatically and lead to an increase in intermicellar distance if the gel volume does not change too much. This is not likely to happen because the intermicellar distance does not have an observable change according to our SANS results. Therefore, we conclude that in the gel state the micellar aggregation number is not sensitive to temperature change. A similar temperature effect also applies to F127 in 1X TBE and D_2O.

SANS studies on aqueous solutions of F127 have been reported by several research groups.[5,7,16,20] Not only were the resulting cubic structures different, but also there existed a controversy regarding the temperature dependence on the aggregation number and the micellar core size in the gel region. The SANS curves obtained by different research groups were actually quite similar. It was the data interpretation which made the conclusion different. This type of discrepancy also happened in the structural studies of the polystyrene−polybutadiene diblock copolymer system.[41,42] The ambiguous peak resolution made the structure determination and reliable model fitting difficult.

SAXS. Figure 10 shows the SAXS intensity patterns of 21.2% F127 in (a) SB and (b) H_2O solutions. The corresponding circular integration profiles are shown in Figure 11. The results are distinct from the usual broad and homogeneous scattering rings obtained from SANS.[7] Instead, bright scattering dots which appeared in several concentric rings can clearly be visualized in the SAXS intensity patterns. In contrast to the SANS

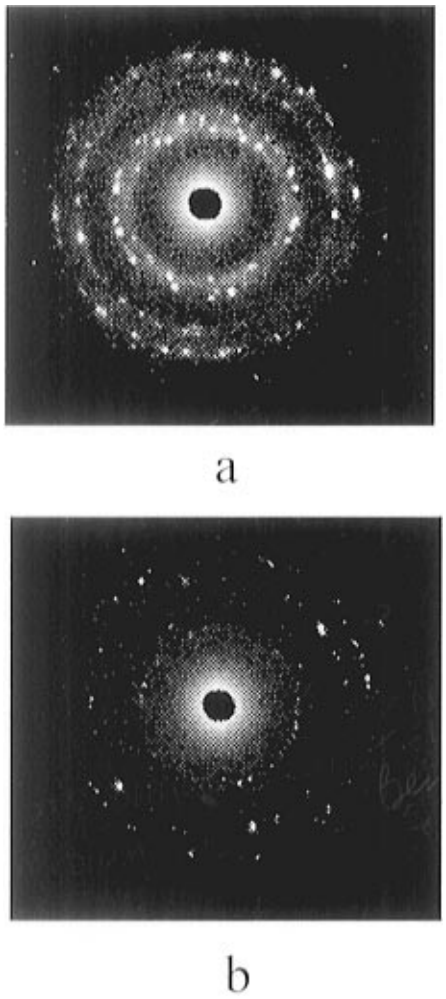

Figure 10. SAXS intensity patterns of 21.2% (w/v) F127 in (a) sequencing buffer and in (b) H_2O solutions at 25 °C.

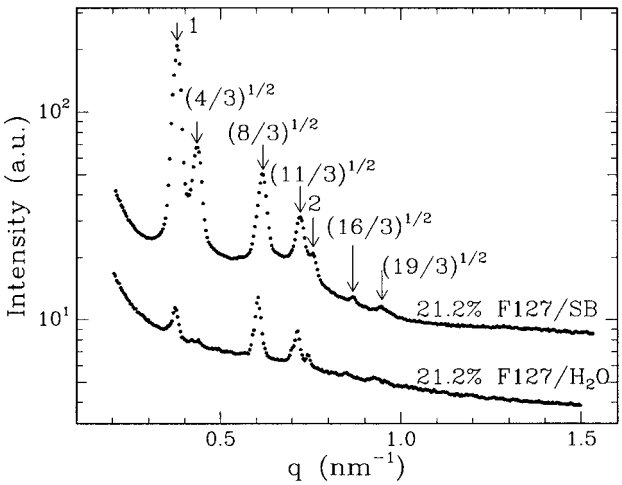

Figure 11. SAXS intensity profiles of 21.2% (w/v) F127 in sequencing buffer and 21.2% (w/v) F127 in H_2O. The arrows indicate peak positions. The numbers represent the ratio of the peak position relative to the first order peak.

profiles in Figures 7−9, the integration profiles in Figure 11 show seven well-resolved peaks with the ratio of relative peak positions being $1:(4/3)^{1/2}:(8/3)^{1/2}:(11/3)^{1/2}:2:(16/3)^{1/2}:(19/3)^{1/2}$. The relatively broader and unresolved peaks obtained by SANS can be attributed to the broader neutron wavelength distribution and neutron beam divergence in the SANS experiment. On the basis of the Bragg diffraction peaks from SAXS we are able

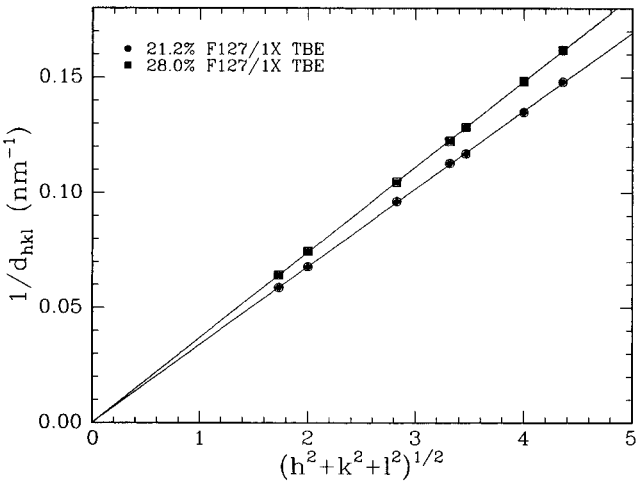

Figure 12. Plot of $1/d_{hlk}$ vm $(h^2 + k^2 + l^2)^{1/2}$, where h, k, l are the Miller indices. Two sets of data points are taken from the peak positions of the SAXS scattered intensity profiles of 21.2% (w/v) and 28.0% (w/v) F127 in 1X TBE buffer solutions. The corresponding Miller indices for the fcc lattice are described in the text. The two straight lines are least-squares linear fittings of the data points.

to determine the F127 gel structure as a face-centered cubic (fcc) latice. The corresponding diffraction planes can also be indexed as (111), (200), (220), (311), (222), (400), and (313). The relation between the interplanar spacing d_{hkl} and the indices hkl for an isometric crystal is

$$d_{hkl} = \frac{a}{\sqrt{h^2 + k^2 + l^2}} \tag{4}$$

where h, k, l are the Miller indices and a is the dimension of a unit cell. Therefore for a fcc structure the plot of $1/d_{hkl}$ vs $(h^2 + k^2 + l^2)^{1/2}$ should result in a straight line with 1/slope = a, passing through the origin. Figure 12 shows such plots for 21.2% F127 and 28.0% F127 in 1X TBE buffer solution, respectively. From the lattice structure and size, we can further calculate the micellar aggregation number N_w for the F127 gel. For the fcc crystal structure, the number density can be described as

$$\rho = 4/a^3 \tag{5}$$

since there are four micelles in one unit cell. ρ can also be calculated from the solution concentration C (w/v), the aggregation number N_w, and the molecular weight of the polymer M_{wt} according to the equation

$$\rho = CN_A/(N_w M_{wt}) \tag{6}$$

where N_A is the Avogadro number. By combining eqs 5 and 6, we can derive the N_w value as

$$N_w = CN_A a^3/(4M_{wt}) \tag{7}$$

By assuming that the micellar core consists of only PPO blocks and that all PPO blocks reside in the micellar core, we can estimate the R_c value by using N_w and the relation

$$(4/3)\pi R_c^3 = N_w M_{wt,PPO}/(N_A \rho_{PPO}) \tag{8}$$

where $M_{wt,PPO}$ is the molecular weight of the PPO block and ρ_{PPO} is the density of PPO. Table 3 lists all the parameters obtained from SAXS. The R_c values calculated from the aggregation number are in agreement with the value estimated from the intraparticle interference form factor. F127 micelles behave slightly different in the gel region in different CE buffers. At the same concentration, the Bragg diffraction peaks result from SB solution tend to shift to higher q values, which led to a smaller intermicellar distance and smaller estimated micellar size. This minor change in the gel region due to the solvent difference is not observed in the SANS experiment mainly because the scattering peaks have been smeared by the broad energy distribution. From the diffraction patterns shown in Figure 10 and the scattering profiles shown in Figure 11, it is very obvious that the micellar cubic crystalline structure in the sequencing buffer is more ordered than that in water or in TBE. The reason is not quite clear at this time. More studies, especially in the dilute solution region, are underway in order to elucidate how the hydrogen bond breaking reagents such as urea and formamide effect the formation of micelles. It is also noted that in Figure 11 the SAXS intensity profile for 21.2% F127 in H_2O has relatively weak first and second order peaks. Similar results can also be found for F127 in 1X TBE buffer as shown in Figure 15. In comparison with their corresponding SANS intensity profiles in Figure 7, the weak first- and second-order peaks in SAXS remain a puzzle even if we take into account the wavelength smearing effect in SANS. However, the disadvantage of the broader wavelength distribution in SANS may be an advantage in terms of the probability of satisfying the Bragg diffraction equation for establishing an effective diffraction intensity, especially for those systems with small crystallite sizes. The $\Delta\lambda/\lambda$ value for our SAXS experiment is on the order of 0.1%. Therefore the limiting condition for diffraction of a given set of planes are more strict. Moreover, by considering the multiplicity factors for the Bragg peaks of a fcc crystal being 8, 6, 12, 24, 8, 6, and 24 for the corresponding peaks indicated in Figure 11 from the first to higher order ones, respectively, the first two peaks do have smaller multiplicity values. For the less ordered structures formed in TBE and H_2O, the relatively weak SAXS intensities for the first two peaks become more reasonable.

Table 3. SAXS Results for F127 gel at 25 °C

C (% (w/v)) solvent	21.2 1X TBE	28.0 1X TBE	21.2 SB	28.2 SB
q_{max} (nm^{-1})	0.369	0.403	0.377	0.414
a (nm)	29.5	27.0	28.8	26.3
N_w	65	66	60	61
R_c (nm)	4.6	4.6	4.4	4.4

Another interesting phenomenon regarding the F127 gel structure is presented in Figure 13. We find that different heating histories for preparing F127 gel in 1X TBE buffer can result in gels with different ordered domain sizes. The corresponding heating curves of Figure 13a,b are shown in Figure 14a,b. A larger ordered domain size can be achieved by slowly bringing the solution from low temperature to room temperature as shown in Figure 13b. The homogeneous rings in Figure 13a indicate a randomly oriented fcc lattice, which is similar to a traditional powder diffraction pattern. Increasing the temperature to 50 °C improves the ordered structure only marginally, as can be seen in Figure 13c,d. By examining the integration profiles in Figure 15 for 21.2% (w/v) F127 in 1X TBE buffer

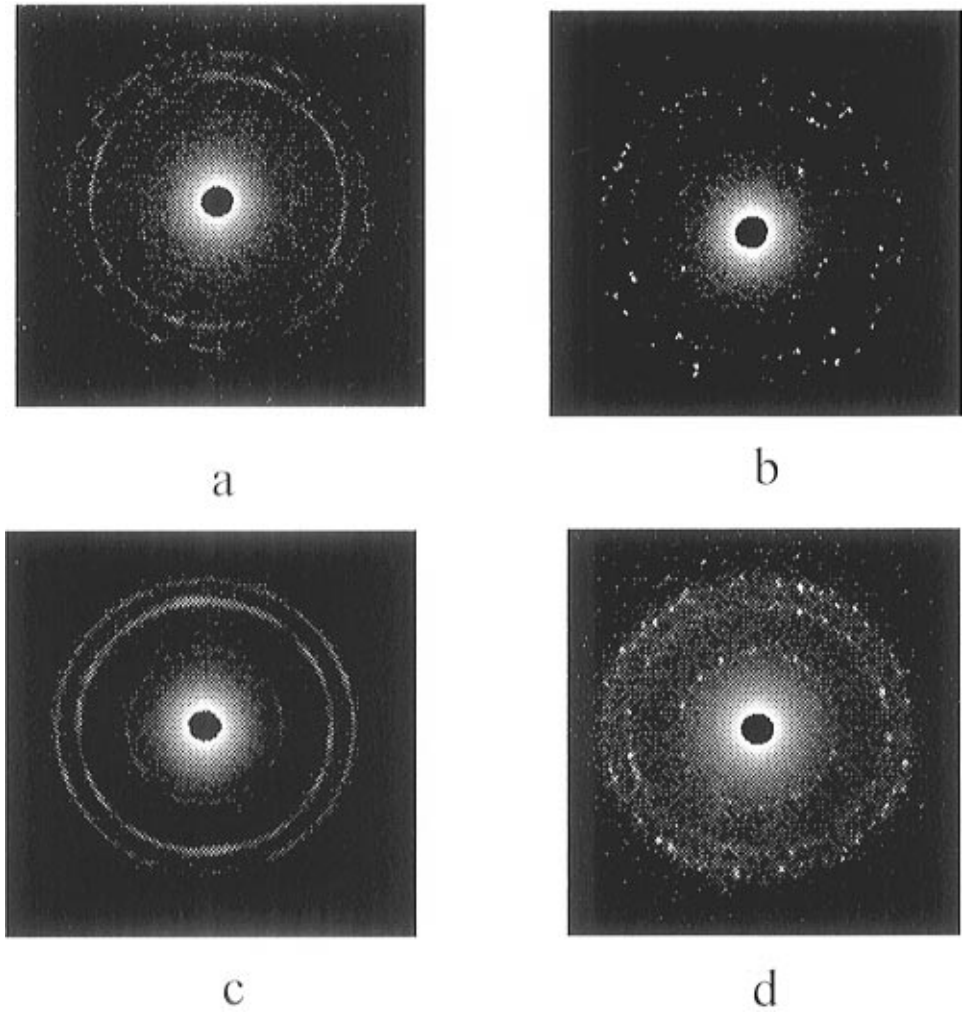

Figure 13. (a and b): SAXS intensity patterns of 21.2% (w/v) F127 in 1X TBE buffer solutions prepared at different heating rates from 4 °C to room temperature. The corresponding heating rates are shown in Figure 14. (c and d) SAXS intensity patterns of samples in (a) and (b) taken at 50 °C.

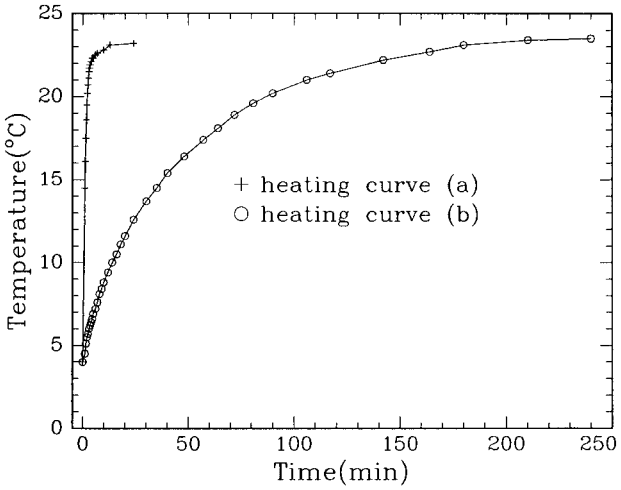

Figure 14. Sample preparation heating curves for the samples in Figure 13a,b.

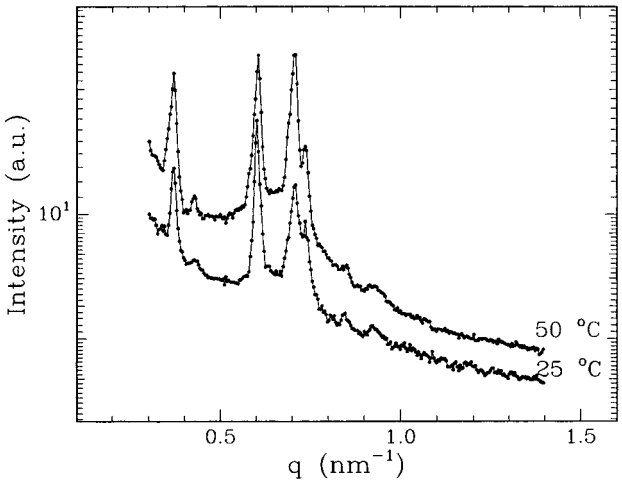

Figure 15. SAXS intensity profiles of 21.2% (w/v) F127 in 1X TBE buffer at (a) 25 °C and (b) 50 °C. The corresponding SAXS intensity patterns are shown in Figure 13b,d.

solution at 25 and at 50 °C, we find similar results as in the SANS experiment; i.e., the diffraction peak positions remain essentially the same. The intensity increase may result from an increase in electron density contrast between the micellar core and the aqueous phase. Figures 13a,c easily show a brighter ring pattern with increasing temperature. The dot pattern in Figure 13b also becomes more distinct after experiencing a temperature increase to 50 °C.

Concentration and Temperature effects on CE Performance. Figure 16 shows a comparison of electropherograms obtained at two different concentrations and temperatures on the F127 gel. With an increase

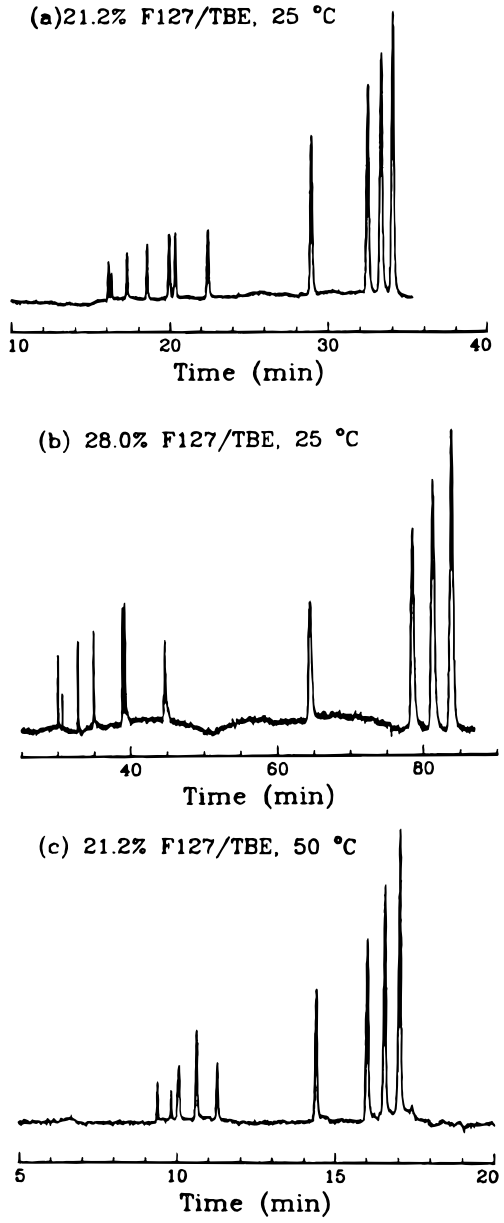

Figure 16. Electropherograms of *ϕX174* DNA-Hae III digest in capillary electrophoresis by using F127 as a separation medium. (a) 21.2% (w/v) F127 in 1X TBE buffer at 25 °C, (b) 28.0% (w/v) F127 in 1X TBE buffer at 25 °C, and (c) 21.2% (w/v) F127 in 1X TBE buffer at 50 °C. Peak identifications from right to left in base pairs are as follows: 1353, 1078, 872, 603, 310, 281, 271, 234, 194, 72, and 118. Electrophoresis conditions are described in the text.

in the gel concentration from 21.2% (w/v) to 28% (w/v), the micellar number density was increased by about 30%. The resulting gel has the ability to retard the DNA electrophoretic migration by a factor of more than 2, as can be seen in Figure 16b when compared with Figure 16a. With an increase in the temperature of the 21.2% (w/v) gel from 25 to 50 °C, the gel lattice parameter and the micellar number density remain about the same as shown by the SAXS and SANS results. The PEO chain will shrink toward the core region when its solubility decreases with increasing temperature which thus results in a decrease in the intermicellar chain entanglement. Some other studies regarding the temperature effect on F127 gel using the fluorescent probe method or NMR[18,25] also drew similar conclusions. These effects can explain the accelerated DNA migration in the gel with increasing temperature as shown in Figure 16c. However, it should also be noted that the resolving power for the smaller DNA fragments is reduced for the separation medium operating at higher temperatures due to a decrease in the supramolecular interchain entanglement.

Conclusions

In this report we demonstrate that Pluronic F127 has the potential to be used as an effective separation medium in capillary electrophoresis for the separation of biomacromolecules such as DNA fragments and proteins. Different scattering techniques have been used to study F127 properties in dilute solution as well as in the gellike regions. LLS results provide us the basic information such as cmc, aggregation number, and hydrodynamic radius in dilute concentration. We do not attempt to compare our results with those in the literature, since there are many discrepancies among the results reported by different research groups. Our emphasis is to examine the structure/property relationship which is relevant to the CE application. At low concentration and low temperature, the 1X TBE buffer is a good solvent for both PPO and PPE blocks. Only the unimer peak is found in the $R_{h,app}$ distribution plot as observed by DLS. Micellar formation can be induced by increasing the temperature or the polymer concentration. In the solution region where micelles dominate, micellar $R_{h,app}$ remains relatively constant although the aggregation number increases with increasing temperature. The micelle has a dense core consisting mainly of PPO and a hydrated PEO shell. At high concentrations, micelles tend to pack into some crystalline structure with relatively well-structured PPO centers. By using a combination of SANS and SAXS results, we are able to conclusively determine the gel structure to have a face-centered cubic lattice. Through the diffraction pattern changes, in terms of peak position, profile intensity, and two-dimensional scattering pattern, we are able to quantitatively calculate and qualitatively elucidate the effects of solvent, polymer concentration, temperature, and sample preparation procedure on the gel structure. F127 behaves very similarly in water and in 1X TBE buffer. The sequencing buffer slightly changes the lattice dimension and the micellar aggregation number in the gellike region. More importantly, F127 micelles form better ordered crystalline domains in the sequencing buffer than in water or TBE. In the gellike region the aggregation number and also the micellar size are not sensitive to the concentration change. Higher concentration only results in closer micellar packing. Intermicellar distance and micellar aggregation number are not sensitive to temperature change. The results of capillary electrophoresis experiments of DNA migration in F127 gel also prove the findings.

Acknowledgment. B.C. gratefully acknowledges support of this work by the National Center for Human Genome Research (Grant 1R01HG0138601), the Department of Energy (Grant DEFG0286ER45237.012), and the Human Frontier Science Program.

References and Notes

(1) Edens, M. W. *Surfactant Sci. Ser.* **1996**, *60*, 185.
(2) Chu, B.; Zhou, Z. *Surfactant Sci. Ser.* **1996**, *60*, 67.
(3) Almgern, M.; Brown, W.; Hvidt, S. *Colloid Polym. Sci.* **1995**, *273*, 2.
(4) Alxandridis, P.; Hatton, T. A. *Colloids Surf. A* **1995**, *96*, 1.

(5) Wanka, G.; Hoffmann, H.; Ulbricht, W. *Colloid Polym. Sci.* **1990**, *268*, 101.
(6) Lenaerts, V.; Triqueneaux, C.; Quarton, M.; Rieg-Falson, F.; Couvreur, P. *Int. J. Pharm.* **1987**, *39*, 121.
(7) Prud'homme, R. K.; Wu, G.; Schneider, D. K. *Langmuir* **1996**, *12*, 4651.
(8) Li, S. F. Y. *Capillary Electrophoresis: principles, practice and applications*; Elsevier: New York, 1992.
(9) Adams, M. A.; Fields, C.; Venter, J. C. *Automated DNA Sequencing and Analysis*; Academic Press: London, 1994.
(10) Grossman, P. D.; Soane, D. S. *Biopolymers* **1991**, *31*, 1221.
(11) Vadnere, M.; Amidon, G.; Lindenbaum, S.; Haslam, J. L. *Int. J. Pharm.* **1984**, *22*, 207.
(12) Malmsten, M.; Lindman, B. *Macromolecules* **1992**, *25*, 5440.
(13) Malmsten, M.; Lindman, B. *Macromolecules* **1993**, *26*, 1282.
(14) Hecht, E.; Hoffmann, H. *Langmuir* **1994**, *10*, 86.
(15) Yu, G.; Deng, Y.; Dalton, S.; Wang, Q.; Attwood, D.; Price, C.; Booth, C. *J. Chem. Soc., Faraday Trans.* **1992**, *88*, 2537.
(16) Mortensen, K.; Talmon, Y. *Macromolecules* **1995**, *28*, 8829.
(17) Rassing, J.; Attwood, D. *Int. J. Pharm.* **1983**, *13*, 47.
(18) Rassing, J.; McKenna, W. P.; Bandyopadhyay, S.; Eyring, E. M. *J. Mol. Liq.* **1984**, *27*, 165.
(19) Attwood, D.; Collett, J. H.; Tait, C. J. *Int. J. Pharm.* **1985**, *26*, 25.
(20) Wanka, G.; Hoffmann, H.; Ulbricht, W. *Macromolecules* **1994**, *27*, 4145.
(21) Malmsten, M.; Lindman, B. *Macromolecules* **1992**, *25*, 5446.
(22) Linse, P.; Malmsten, M. *Macromolecules* **1992**, *25*, 5434.
(23) Linse, P. *Macromolecules* **1993**, *26*, 4437.
(24) Alexandridis, P.; Holzwarth, J. F.; Hatton, T. A. *Macromolecules* **1994**, *27*, 2414.
(25) Gilbert, J. C.; Washington, C.; Davies, M. C.; Hadgraft, J. *Int. J. Pharm.* **1987**, *40*, 93.
(26) Wu, C.; Quesada, M. A.; Schneider, D. K.; Farinato, R.; Studier, F. W.; Chu, B. *Electrophoresis* **1996**, *17*, 1103.
(27) Wang, Z. L.; Chu, B.; Wang, Q.-W.; Fetters, L. *New Trends in Physics and Physical Chemistry of Polymers*; Plenum: New York, 1989.
(28) Chu, B.; Harney, P. J.; Li, Y.; Linliu, K.; Yeh, F.; Hsiao, B. S. *Rev. Sci. Instrum.* **1994**, *65*, 597.
(29) Schmolka, I. R. *J. Am. Oil Chem. Soc.* **1991**, *68*, 206.
(30) Laemmli, U. K. *Proc. Natl. Acad. Sci. U.S.A.* **1975**, *72*, 4288.
(31) Minagawa, K.; Matsuzawa, Y.; Yoshikawa, K.; Khokhlov, A. R.; Doi, M. *Biopolymers* **1994**, *34*, 555.
(32) Harris, J. M. *Topics in Applied Chemistry: Poly(ethylene glycol) Chemistry, Biotechnical and Biomedical Applications*; Plenum Press: New York, 1992.
(33) Stellwagen, N. C. *Biochemistry* **1983**, *22*, 6186.
(34) Berka, J.; Pariat, Y. F.; Muller, O.; Hebenbrock, K.; Heiger, D. N.; Foret, F.; Karger, B. L. *Electrophoresis* **1995**, *16*, 377.
(35) Zhou, Z.; Chu, B.; Nace, V. M. *Langmuir* **1996**, *12*, 5016.
(36) Provencher, S. W. *Biophys. J.* **1976**, *16*, 29; *Chem. Phys.* **1976**, *64*, 2772.
(37) Alexandridis, P.; Nivaggioli, Hatton, T. A. *Langmuir* **1995**, *11*, 1468.
(38) Mortensen, K.; Pedersen, J. S. *Macromolecules* **1993**, *26*, 805.
(39) Glatter, O.; Scherf, G.; Schillen, K.; Brown, W. *Macromolecules* **1994**, *27*, 6046.
(40) Bates, F. S.; Cohen, R. E.; Berney, C. V. *Macromolecules* **1982**, *15*, 589.
(41) Shibayama, M.; Hashimoto, T.; Kawai, H. *Macromolecules* **1983**, *16*, 16.
(42) Harkless, C. R.; Singh, M. A.; Nagler, S. E.; Stephenson, G. B.; Jordan-Sweet, J. L. *Phys. Rev. Lett.* **1990**, *64*, 2285.

MA9701088